ELSEVIER

Automation in Construction 15 (2006) 58 – 72

AUTOMATION IN CONSTRUCTION

www.elsevier.com/locate/autcon

Automated detection of cracks in buried concrete pipe images

Sunil K. Sinha [a,*], Paul W. Fieguth [b]

[a] Department of Civil and Environmental Engineering, Pennsylvania State University, University Park, PA 16802, USA
[b] Department of Systems Design Engineering, University of Waterloo, Ontario, Canada N2L3G1

Accepted 4 February 2005

Abstract

The detection of cracks in concrete infrastructure is a problem of great interest. In particular, the detection of cracks in buried pipes is a crucial step in assessing the degree of pipe deterioration for municipal and utility operators. The key challenge is that whereas joints and laterals have a predictable appearance, the randomness and irregularity of cracks make them difficult to model. Our previous work has led to a segmented pipe image (with holes, joints, and laterals eliminated) obtained by a morphological approach. This paper presents the development of a statistical filter for the detection of cracks in the pipes. We propose a two-step approach. The first step is local and is used to extract crack features from the buried pipe images; we present two such detectors as well as a method for fusing them. The second step is global and defines the cracks among the segment candidates by processes of cleaning and linking. The influences of the parameters on crack detection are studied and results are presented for various pipe images.

Keywords: Pipeline Infrastructure; Automated inspection; Pipeline assessment; Image processing; Segmentation; Crack detection; Statistical properties

1. Introduction

Segmentation of pipe images aims at the separation of distresses (if any) from the image background. Thus, as a result of the segmentation process, each image pixel is classified into two categories: healthy (background) and distress (other). We have previously developed a morphological approach to the segmentation problem [1], as shown in Fig. 1. Experimental results have demonstrated that the proposed approach is effective in segmenting holes, joints, laterals and pipe collapse. However, the segmentation and classification of cracks in a pipe surface (the focus of this paper) is particularly difficult because of the irregularities in crack shape and size, the background camouflage of corroded areas, debris, patches of repair work, and areas of poorly illuminated conditions.

Crack detection is of broad interest and has been studied extensively because a wide variety of civil structures can crack (roads, bridges, pipes, pillars, columns, beams, etc.), and an assessment of cracking may be crucial for reasons of safety and cost-effective maintenance. Indeed, many researchers have paid a great deal of attention to automated cracking detection/classification. Li et al. [2] proposed an algorithm for pavement cracking detection based on certain histogram assumptions. A standard model was proposed to represent pavement surface images toward a unified and automated acquisition of key characteristics for improving data quality [3]. However, this model did not discuss how to employ such a mode in crack detection/classification system. An approach to the recognition of segmented pavement distress images was studied in Mohajeri and Manning [4]. It uses directional filters to classify the cracks. The crack is longitudinal if there is a high concentration of object pixels in a narrow interval of x (transverse) coordinates, and it is transverse if there is a high count of object pixels in a narrow interval of y (longitudinal) coordinates. However, it is difficult to get a segmented crack image, and it is also not clear how to identify other crack types by analyzing these counts. Another statistical approach [5] recognized the imperfec-

* Corresponding author. Tel.: +1 814 865 9433; fax: +1 814 863 7304.
E-mail addresses: sunil@engr.psu.edu (S.K. Sinha), pfieguth@uwaterloo.ca (P.W. Fieguth).

0926-5805/$ - see front matter © 2005 Elsevier B.V. All rights reserved.
doi:10.1016/j.autcon.2005.02.006

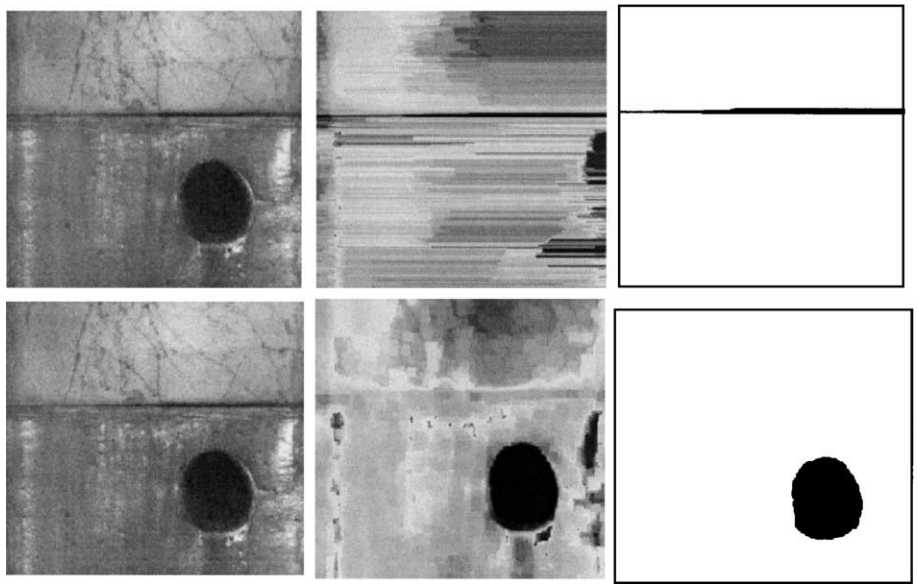

Fig. 1. A morphological approach [1] to joint/lateral discrimination using different structuring elements: a horizontal element (top) of length 285 mm, consistent with the geometry of a joint, as opposed to a circular element (bottom) of radius 57 mm, tuned to the shape of a lateral.

tions of segmentation that cause difficulty in distinguishing pavement-cracking types, particularly between multiple and mushroom cracks. In this method, the original image is enhanced by subtracting an average of a few plain (non-distress) images from the same series to compensate for the lighting variations. A crack is detected by assigning one out of four values to each pixel, based on its probability of being an object pixel. Regazzoni [12] defines a cooperative process between three levels of a Bayesian network [21], allowing the introduction of local contextual knowledge as well as more global information concerning straight line. Hellwich [13] uses Bayesian a priori information concerning line continuity expressed as neighborhood relations between pixels.

Interest in crack-like features is far broader than civil infrastructure, and many approaches have been developed to deal with the detection of linear features such as road networks in satellite images, arteries in retinal images, bone structures, cell boundaries, etc. [5–11]. Nearly all of these methods approach crack/line detection similarly, as a local spatial operator, seeking narrow regions (cracks) whose statistics are at odds with the surroundings (background). By adjusting this detector over position, size and orientation, cracks of different sizes and angles may be found. The approach proposed in this paper builds on these methods, and the experimental performance is found to be in good agreement with the manual detection of cracks.

2. Proposed statistical filters for crack detection

We propose a two-step algorithm for the detection of crack features in the segmented underground pipe images. The first step is local and uses statistical properties to extract crack features from the segmented image, which are treated as crack segment candidates. In the second step, global cleaning and linking operations merge segments to form cracks.

The algorithm begins by performing a local detection of cracks, based on the fusion of the results from two crack detection filters, both taking the statistical properties of image into account. The first crack detector D_1 is based on a ratio edge detector: An in-depth statistical study of its behavior is given in Lopes et al. [9]. The second crack detector D_2, which has emerged from this research, uses the operators of Yakimovsky [10]. Responses from both the first and second detectors are merged to obtain a unique response as well as an associated direction in each pixel. The detection results are post-processed to provide candidate segments. Fig. 2 shows the different steps of the proposed crack detection algorithms.

Both detectors are based on the same basic model, considering the relative statistics of those adjacent regions R_1, R_2, and R_3 as shown in Fig. 3. We denote by $|R_i|$, μ_i, σ_i^2 the number of pixels, sample mean, and sample variance over R_i.

2.1. Crack detector D_1

The ratio crack detector is defined as the ratio of the average of pixel values of two non-overlapping adjacent neighborhoods. The response of the detector between region i and j is defined as

$$r_{ij} : r_{ij} = 1 - \min\left(\mu_i/\mu_j, \mu_j/\mu_i\right) \tag{1}$$

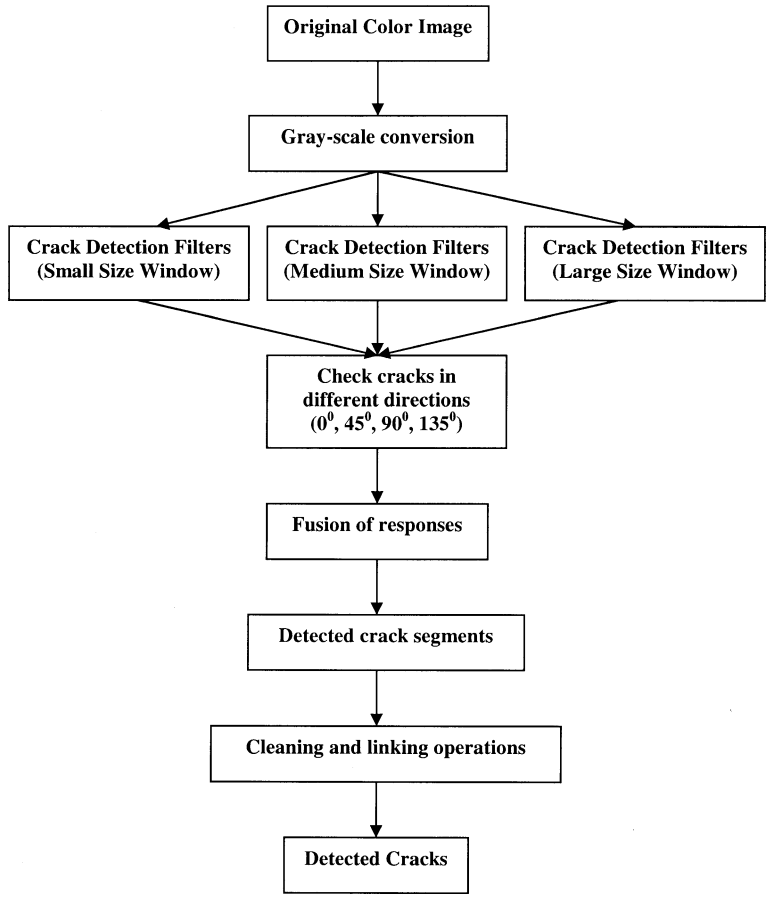

Fig. 2. The proposed method for crack detection in underground pipe images.

thus, the overall response is

$$D_1 = \min(r_{12}, r_{13}) \tag{2}$$

the minimum response of the ratio crack detector on both sides of the hypothesized crack structure. Implicitly, D_1 is a function of location (x,y) and of model parameters $(l,\ m,\ n,\ \theta)$. With detector D_1, a pixel is considered as belonging to a crack when its response is large enough, i.e., higher than some a priori chosen threshold τ_1.

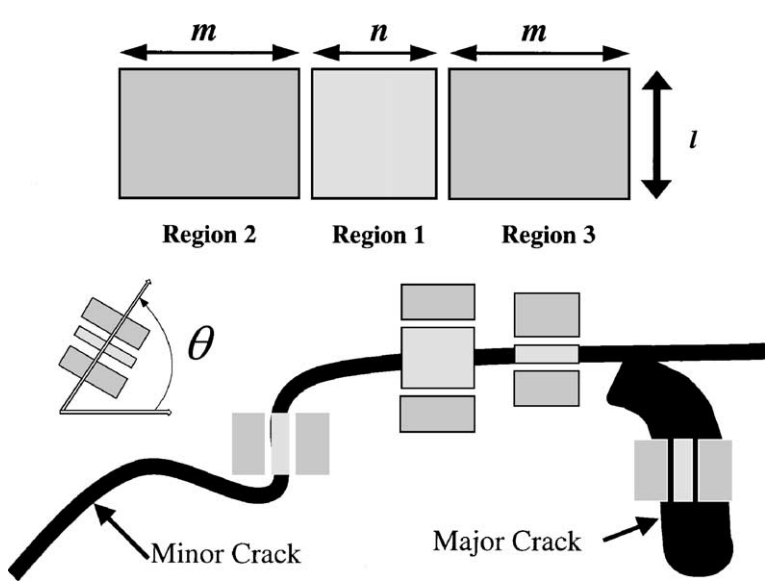

Fig. 3. Crack model used by the two crack detectors D_1 and D_2.

2.2. Crack detector D_2

In practice, the ratio crack detector D_1 is accurate, but only the mean comparison component behaves well when the operator is not centered on an edge interface. Therefore, we decided to use the variance comparison also as suggested by Yakimovsky [10]. The operators of Yakimovsky assume that cracks are interfaces between sets of points, each set being described by a normal distribution. The mathematics for distribution parameter comparison is used to form a function of crack strength in an area.

The resulting discriminate D_2 is

$$D_2 = \left[\frac{\left(\sigma_0^2\right)^{|R_0|}}{\left(\sigma_1^2\right)^{|R_1|}\left(\sigma_2^2\right)^{|R_2|}} \right] \tag{3}$$

where σ_0^2 is the sample variance over the combined region $R_0 = R_1 \cup R_2 \cup R_3$, and where absolute value is the number of pixels in region R.

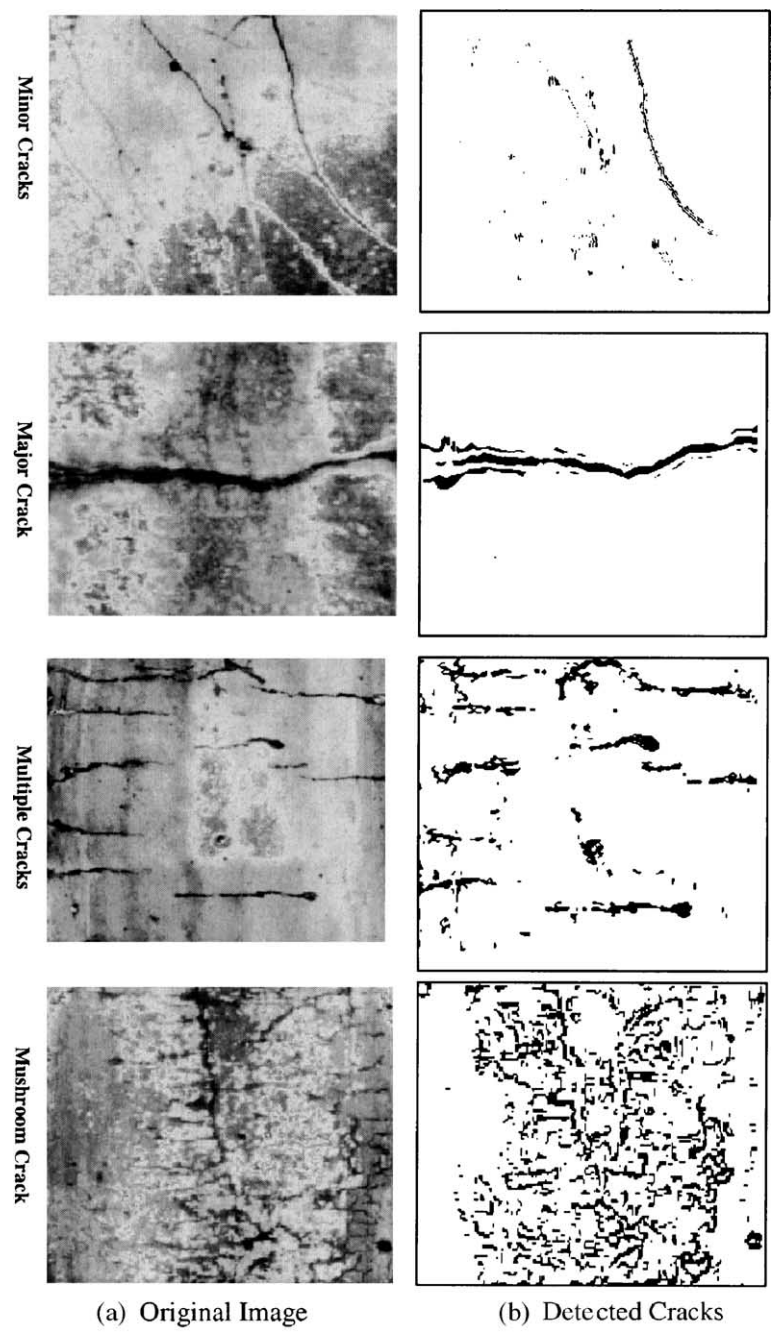

Fig. 4. Crack detection filters response before cleaning and linking operations.

A pixel is considered as belonging to a crack when its response D_2 is large enough, i.e., higher than some a priori chosen threshold τ_2.

2.3. Fusion of responses

In the previous sub-sections, we have addressed the problem of detection of cracks in the segmented pipe images, using two detectors D_1 and D_2. Since there does not appear to exist a single detector suitable for reliable detection of cracks, we decided to merge information from both D_1 and D_2 by using an associative symmetrical sum, as defined in [14]:

$$\text{Fused Response} f(D_1, D_2) = \frac{D_1 D_2}{1 - D_1 - D_2 + 2D_1 D_2}, \text{ with } D_1, D_2 \in [0, 1] \quad (4)$$

This fusion operator has been chosen because of its indulgent disjunctive behavior for high values ($D_1 > 0.5$, $D_2 > 0.5$), its severe conjunctive behavior for small values ($D_1 < 0.5$, $D_2 < 0.5$), and its adaptive behavior in other cases.

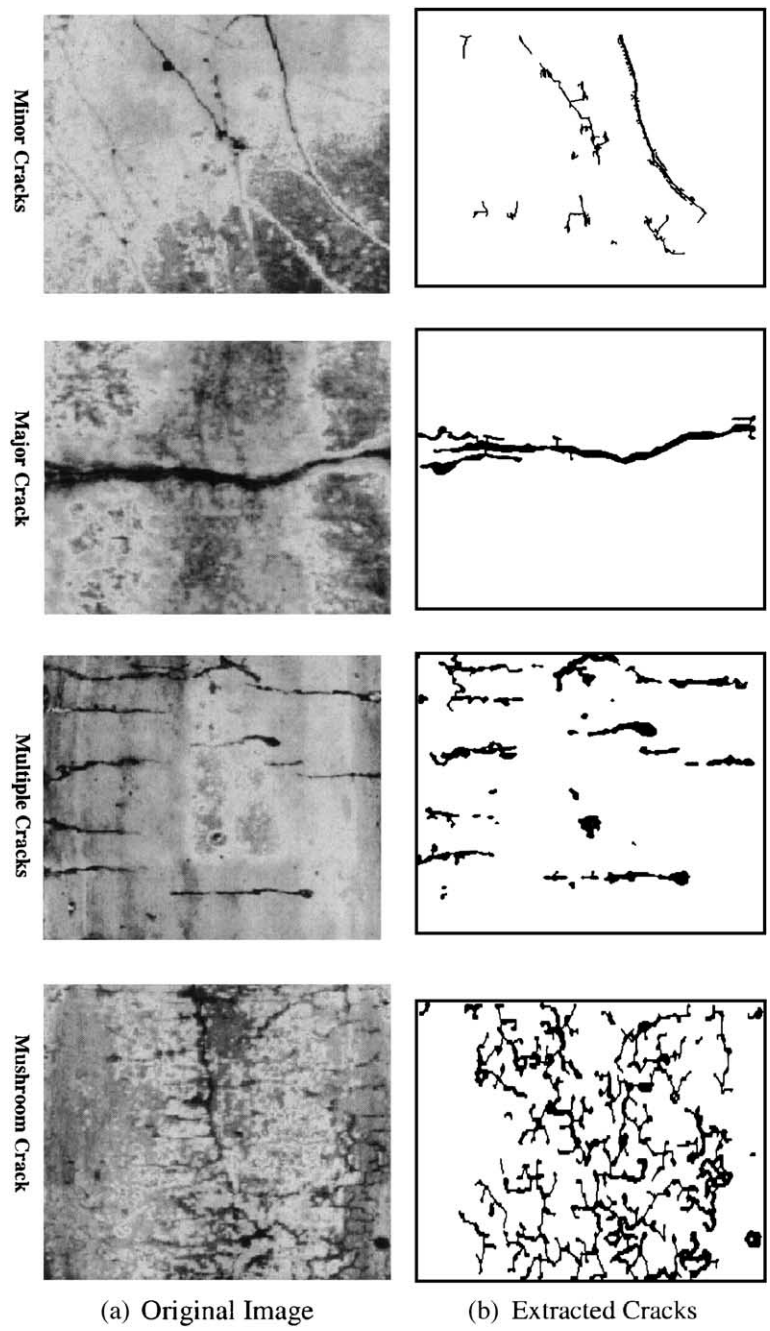

Fig. 5. Filters response after cleaning and linking operations.

Since the behavior of this operator depends on the position of the responses compared to the value 0.5, we first centered both D_1 and D_2 responses before applying the fusion, so that the decision threshold corresponds to 0.5. In order to do so, and constraining the values to lie in the interval [0,1], we replace $\bar{D}=\max[0, \min(1, D+0.5-D_{\min})]$, so the fused response becomes $f(\bar{D}_1, \bar{D}_2)$. As a result, the decision threshold applied on f is automatically the central value 0.5 of the interval [0,1].

To detect most of the cracks, the operators must be applied in all possible directions. If the operator is applied separately for each direction, the same threshold must be used for all the considered directions. In this study, we found it appropriate to limit consideration to four directions (0°, 45°, 90°, 135°) for the detection of cracks. The response image is thresholded with a threshold of 0.5, resulting in a binary image. The thresholded response from the crack detector is shown in Fig. 4. As seen in Fig. 4(b), the image contained many disjointed crack segments and noise. A necessary step for all detection methods based on local detectors is a non-local linking process.

2.4. Cleaning and linking operations

No detection method is perfect, in the sense that it finds all crack pixels and only crack pixels. Usually, unwanted noise is present in the form of short, erratic edges, and some crack pieces remain disconnected from other pieces by gaps. Both of these problems are addressed in the cleaning and linking process.

As with crack detection, linking methods may be local or global. Local methods deal with a neighborhood around the pixel to be linked, analyzing the characteristics of these neighboring pixels to determine where the links should be. The simplest of local schemes focus on a small neighborhood and use information from earlier edge detection in order to find pixels with similar characteristics. As the size of the neighborhoods gets larger, searches are introduced based on a variety of path metrics [15]. Fuzzy reasoning has also been used to deduce which pixels in the search area should be linked together [16]. Global methods look at the overall pattern of cracks and try to describe the features using few variables, for example, modeling the crack image as a potential function [17], using a Hough transform [18], Markov random fields [19], or least-square-error curve fitting [20].

The linking procedure that follows in this study is local and specifically focuses on linking pixels that represent cracks. That is, we wish to assert a prior model—cracks are usually long and relatively thin—to influence which neighborhoods are searched for points to link together. A hierarchical clustering technique [21] is used for linking small gaps and removing unwanted noise (short, isolated). The nearest neighbor [21] similarity measure is used in clustering because it is naturally well suited to extract string-like clusters.

The first step in the linking process is to establish which crack points are end points and the direction in which the crack is heading. Once this is established, the crack clusters are linked if the distances between their end points are less than 15 pixels (a gap size selected empirically). Steps are taken to connect end points of each cluster only once. In this manner, links are made that fill small gaps in crack segments. This also allows some of the noise to be eliminated by deleting isolated clusters with few pixels. The filter response after cleaning and linking operations is shown in Fig. 5.

The linking method can be further improved if special cases are accounted for. Linking only takes place between end points, ignoring the fact that other crack points may provide a better starting point for linking. The links are made with straight lines, neglecting the possibility that the crack may be in the process of curving. Overall, some crack gaps may be missed and some false links may be made. Nonetheless, provided that enough cracks are kept in the crack detection stage, this linking process will fill most of the gaps that should be filled and remove some of the noise.

3. Detector parameter estimation

We have applied the crack detector to 250 underground concrete sewer pipe images with or without cracks, images obtained from SSET inspection of flush cleaned concrete sewer pipes 18 in. in diameter from various municipalities in North America. The characteristics of the data set are summarized in Table 1. The evaluation of crack detection is carried out by comparing the automatically detected cracks with ground truth from manual crack extraction as shown in Fig. 6. The purpose of this evaluation is to estimate the model parameters (l, m, n of Fig. 3).

Table 1
Characteristics of the pipe image data set for evaluation of crack detection filter

City	Clean pipe	Transverse crack	Longitudinal crack	Diagonal crack	Multiple crack	Mushroom crack
Los Angeles	15	15	10	7	15	5
Toronto	15	5	12	2	20	3
Boston	15	12	8	3	10	2
Washington, DC	15	8	5	5	10	3
Albuquerque	15	5	0	3	5	2

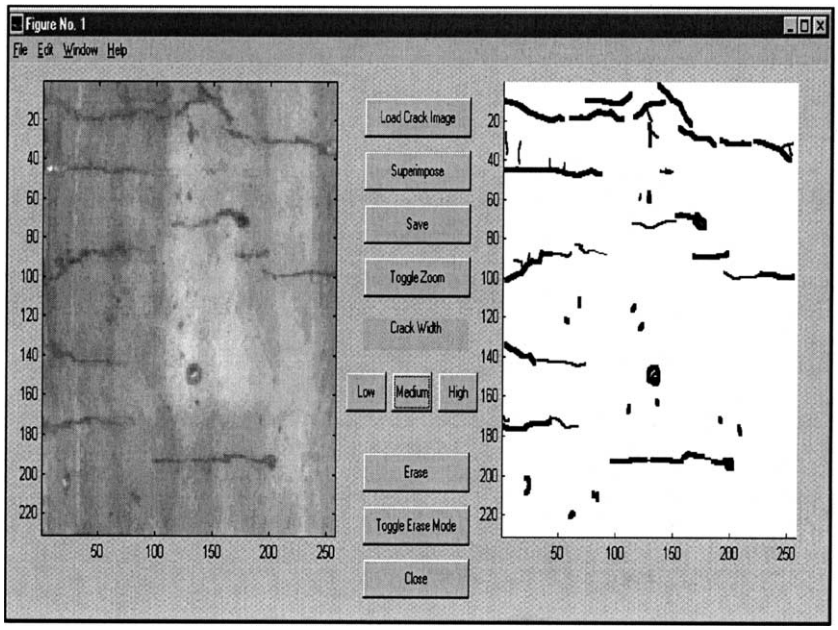

Fig. 6. Software for extraction of crack reference map for evaluation of the proposed crack detection filters; original crack image is shown on the left side of the window and the manually plotted crack reference map on the right window.

We will assess the matching between hand labeling and automatic extraction using a 'buffer method' [22], a simple matching procedure in which a buffer of constant predefined width is constructed around the crack data in two steps. In the first step, a buffer of constant width is constructed around the ground truth data using a morphological dilation operation as shown in Fig. 7(a). The parts of the extracted data within the buffer are considered as matched and are denoted as true positive; the unmatched extracted data are denoted as false positive. In the second step, matching is performed the other way, a buffer now constructed around the extracted crack data, as shown in Fig. 7(b), and the part of the reference data lying in the buffer is considered as matched. The unmatched reference data is denoted as false negative. Fig. 8(a–i) illustrates this matching procedure.

Let C_f be the set of pixels detected as crack pixels in the image filtered by filter f, and C_t the set of true crack pixels, extracted manually by the experts and $d(\ )$ the morphological dilation by some structuring element. Then the pixel sets of interest are

$$S_1 = C_f \cap d(C_t) \quad \text{(true positive)}$$
$$S_0 = C_f \cap \text{not } d(C_t) \quad \text{(false positive)}$$
$$S_3 = C_t \cap d(C_f) \quad \text{(true positive)}$$
$$S_4 = C_t \cap \text{not } d(C_f) \quad \text{(false negative)}$$

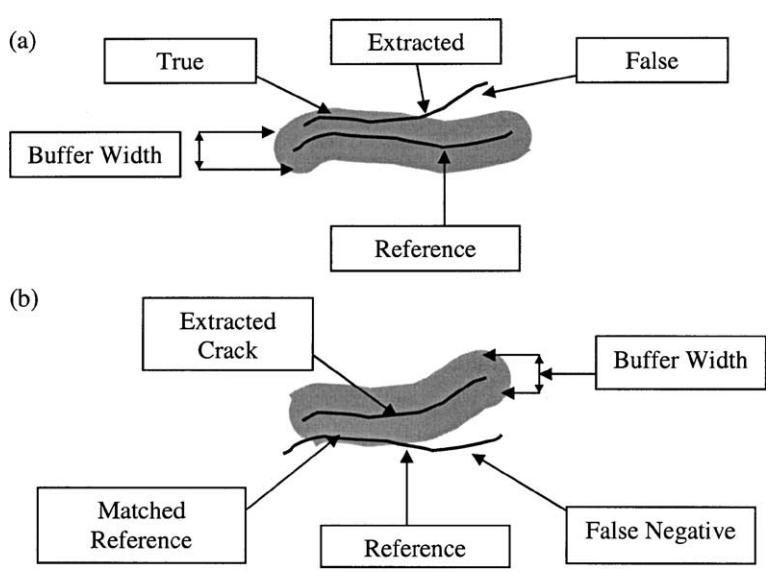

Fig. 7. Matching principle for the evaluation of crack detector responses. (a) Matched extracted. (b) Matched reference.

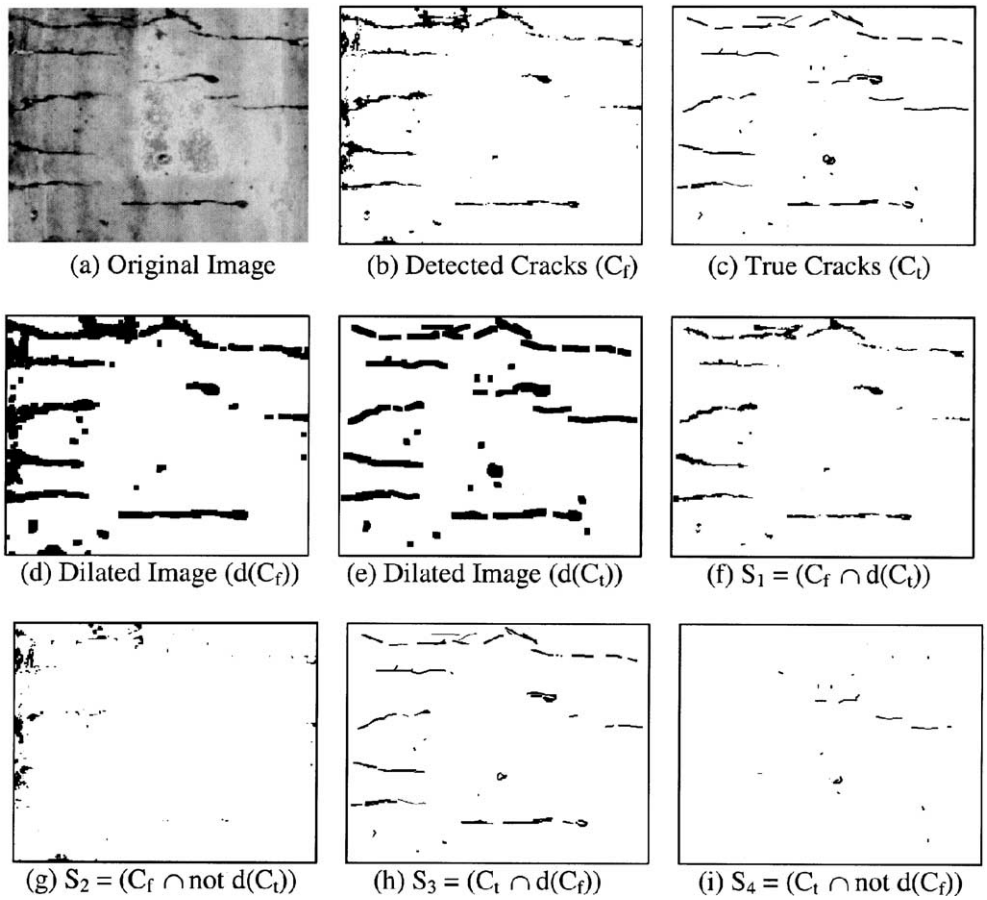

Fig. 8. Illustration of the procedure of matching the images for detection of true and false pixels.

Now, the probability of detection (P_d) and false-alarm (P_{fa}) can be defined as follows:

$$P_d = \frac{\text{Number of detected crack pixels}}{\text{Number of true crack pixels}}; \quad P_d = \frac{|S_3|}{|C_t|} \tag{5}$$

$$P_{fa} = \frac{\text{Number of false} - \text{alarm pixels}}{\text{Number of non} - \text{crack pixels}};$$

$$P_{fa} = \frac{|S_2| + |S_3|}{|I|} \tag{6}$$

where $|I|$ are the numbers of pixels in the whole image I.

Thus, we can quantify the performance of the crack detectors as a function of the detector parameters: size of neighborhood and decision threshold. The probability of detection (P_d) is plotted against the probability of false alarm (P_{fa}), optimizing the widow size, over parameter sets l=3, 5, 7, 9, 11, 13, 15, m=3, 5, 7, 9, 11, and n=2, 3, 4, 5, 6, 7. As would be expected, it was found that larger neighborhoods reduced noise sensitivity, but increased the probability that small cracks would be missed. Therefore, in order to maximize crack detection, the filters must operate over neighborhoods of different sizes. Three sizes of crack detection filters are selected based on empirical Receiver Operating Characteristic (ROC) curves [16] for detecting various cracks.

An ROC curve summarizes the range of tradeoffs between true positive and false positive crack pixels, as determined by comparing the detected crack pixels to the specified ground truth. ROC curves are plotted as a function of P_d and P_{fa} for different neighborhood sizes. As an example, ROC curves for neighborhood size (m=5, n=3, l=7) are shown in Fig. 9(a–c). As usual, the detection probability (P_d) decreases and the false-alarm rate (P_{fa}) increases as the threshold increases. The threshold τ_1, τ_2 may be deduced as a compromise between P_{fa} and P_d.

In this study, P_{fa} is selected as 9% (7% false-positive and 2% false-negative) as suggested by municipal engineers and thus determining the threshold value, the corresponding window size is selected which gives the maximum P_d value. This process is repeated for the three different classes of cracks: minor, major and multiple cracks. Therefore, three optimal sizes of windows and the corresponding threshold values τ_1 and τ_2, as shown in Table 2, are used for detection of cracks in underground pipe images.

4. Conventional techniques for crack detection

To study the performance of proposed crack detection filters, we propose to compare them with conventional

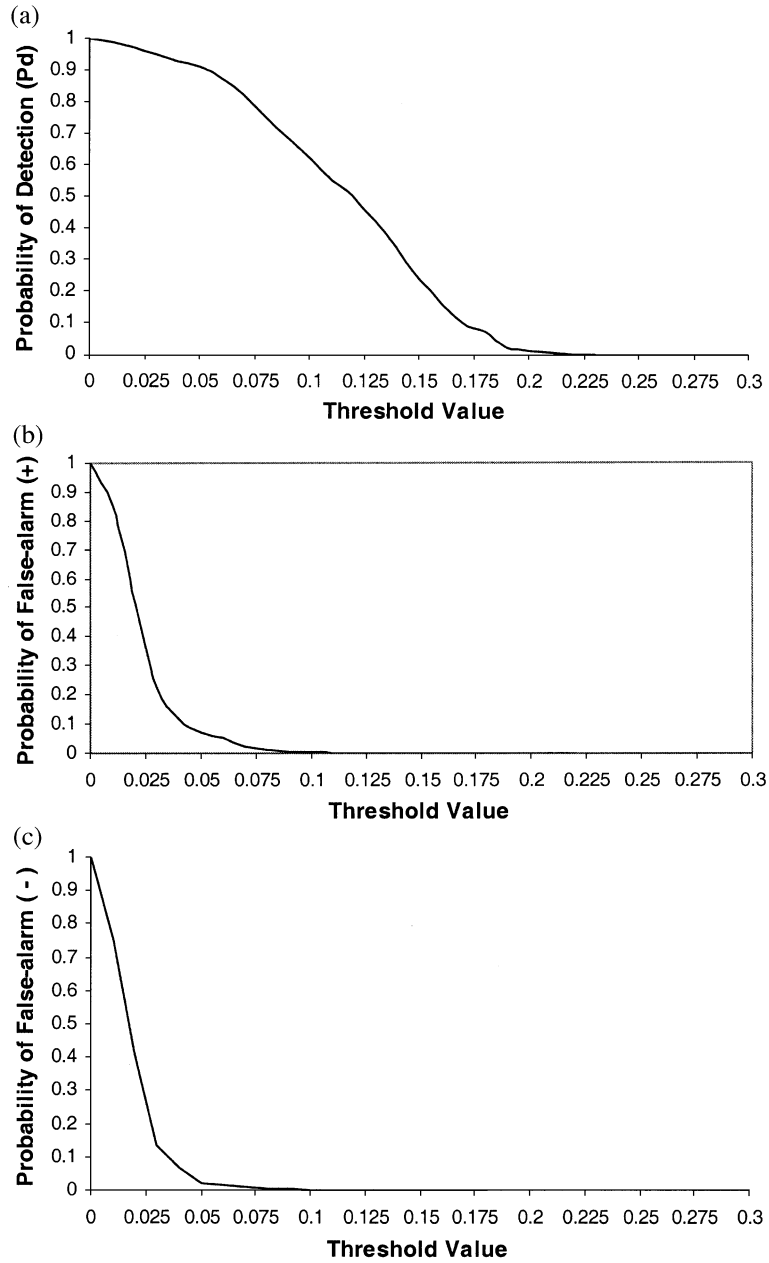

Fig. 9. (a) Probability of detection vs. the minimum threshold value of crack detection filter. (b) Probability of false alarm (positive) vs. the threshold value of crack filter. (c) Probability of false alarm (negative) vs. the threshold value of crack filter.

techniques: Canny's edge detector [23] and Otsu's thresholding [24]. The Canny operator is used because it can perform very well in detecting edges due to intensity changes. It is known for emphasizing weak edges and yet suppressing edge output due to noise. Otsu's thresholding method is selected because it is non-parametric, unsupervised and automatic. The following sub-sections will briefly discuss these techniques.

4.1. Canny edge detection

Edge-detection techniques segment objects by outlining their boundaries using information on gray-scale discontinuity. This step, however, seldom produces connected object edges due to noise and other factors. Thus, edge linking and other boundary detection methods usually follow to transform the set of edge pixels obtained into a

Table 2
Optimal window size for central and adjacent regions with threshold values for crack detection filters

Filter size	m	n	l	τ_1	τ_2
Small	3	2	5	0.05	0.15
Medium	5	3	7	0.1	0.25
Large	7	5	11	0.175	0.35

meaningful set of object boundaries. The Canny edge detector [23] uses linear filtering with a Gaussian kernel to smooth the noise in the image. Next, the edge strength and direction are calculated for every pixel by differentiating the image in the horizontal and vertical directions and computing the gradient magnitude and direction. The next step, non-maximal suppression, sets the edge strength of each candidate edge pixel to zero if its edge strength is not larger than those of the two adjacent pixels in the gradient direction. The pixels that survive the non-maximal suppression thinning process are labeled as candidate edge pixels. An adaptive thresholding method is then applied on the thinned edge magnitude image to obtain the final edge map.

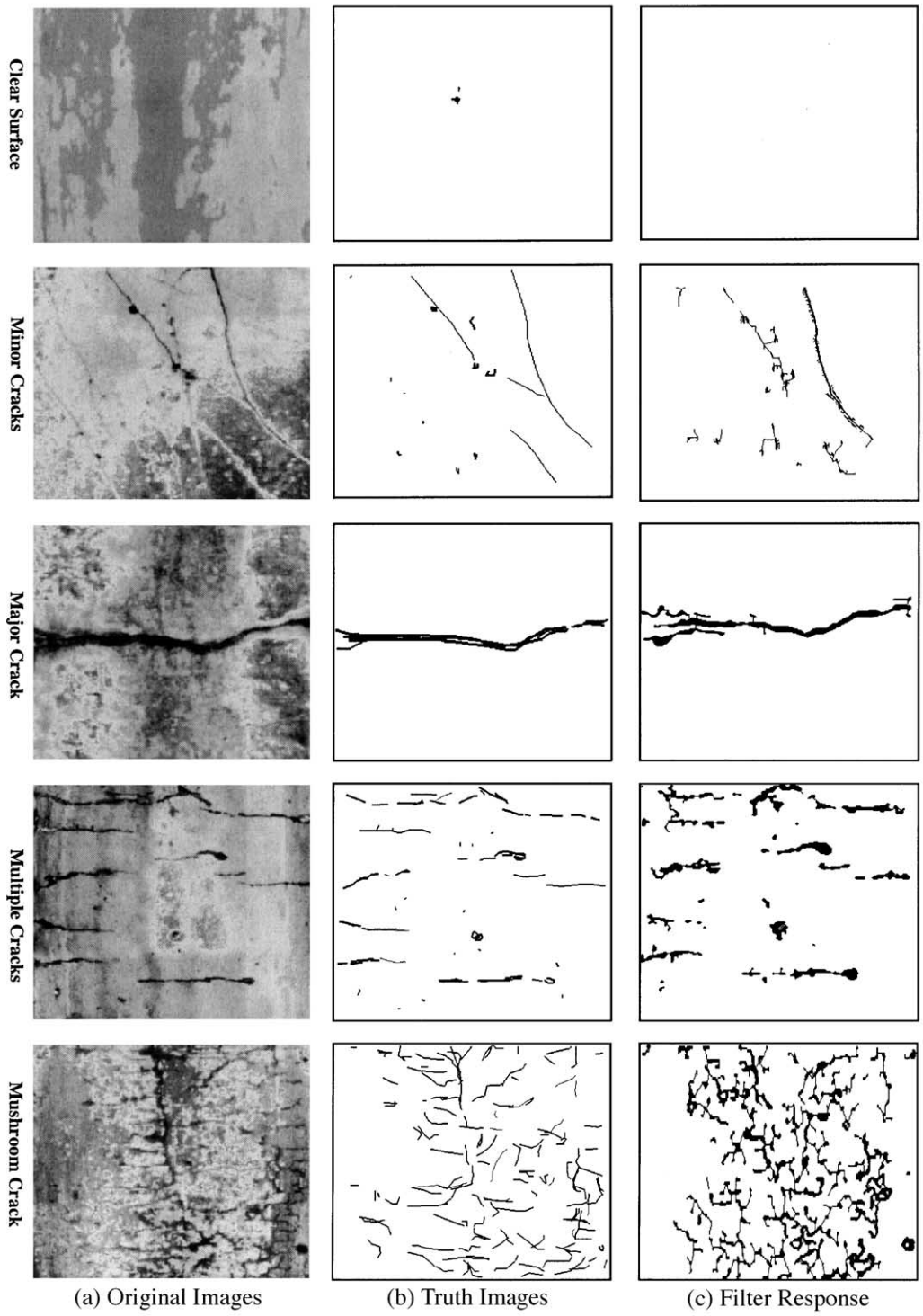

Fig. 10. Crack detection filters response after cleaning and linking operations.

4.2. Otsu's thresholding

The Otsu method [24] is an automated and unsupervised method of thresholding using gray-level histograms. A discriminant criterion between two classes of pixels is computed for each possible threshold k; the optimal threshold is that gray level where this measure is maximized. It has the advantages that it is simple and easy to implement and the threshold thus selected is not based on the differentiation (a local property) but rather on the integration (a global property) of the histogram. As a result, the criterion measure is always unimodal and stable. Given V gray levels $\{0, 1, 2, \ldots, V-1\}$, let the number of pixels in gray level v be denoted by n_v and the total number of pixels

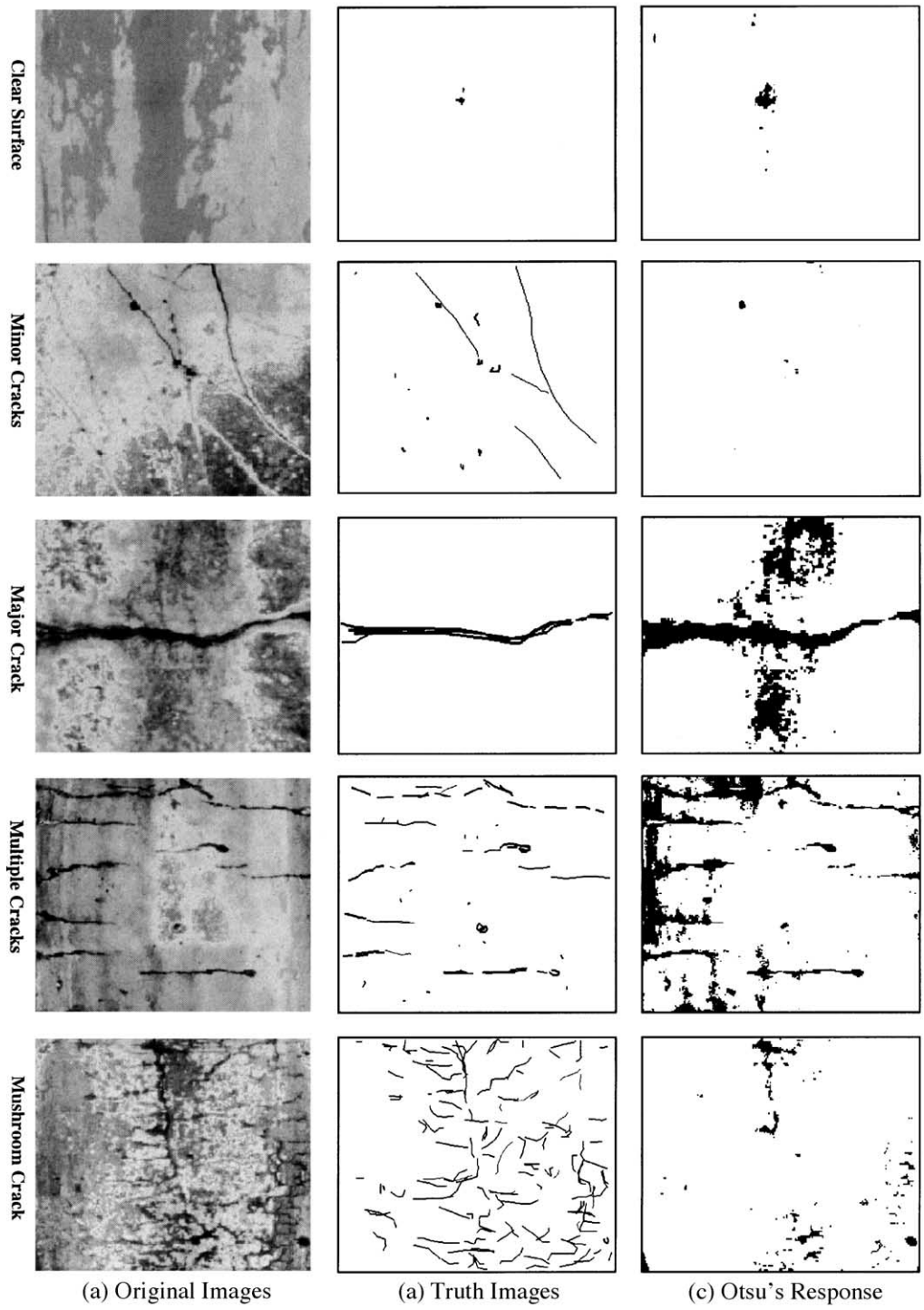

Fig. 11. Otsu's method response.

be N. To simplify, the gray-level histogram is normalized and regarded as a probability distribution function:

$$P_v = \frac{n_v}{N} \qquad P_v \geq 0 \qquad \sum_{V=0}^{V-1} P_v = 1 \quad \mu_T = \sum_{V=0}^{V-1} vP_v \tag{7}$$

Suppose we divide the pixels into two classes C_0 and C_1 (background and object) by a threshold value at k. Then probabilities of class occurrences ω and class mean levels μ for both classes are given by

$$\omega_0 = \sum_{V=0}^{k} P_v \quad \text{and} \quad \mu_0 = \frac{1}{\omega_0} \sum_{V=0}^{k} vP_v \tag{8}$$

$$\omega_1 = \sum_{V=k+1}^{V-1} P_v \quad \text{and} \quad \mu_1 = \frac{1}{\omega_1} \sum_{V=k+1}^{V-1} vP_v \tag{9}$$

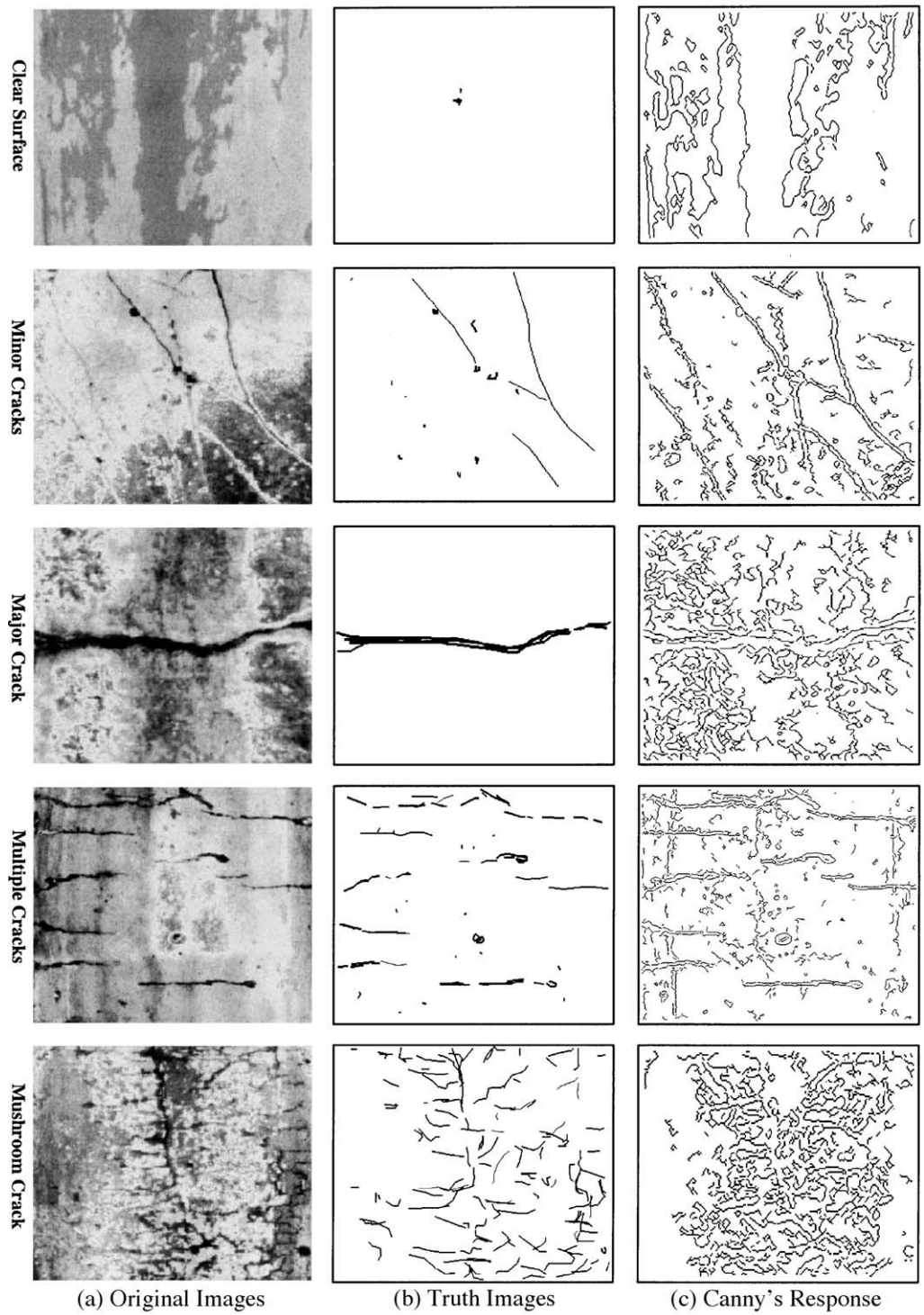

Fig. 12. Canny's method response.

Table 3
Comparison under completeness metric (ideal response=1)

Methods	Minor cracks	Major cracks	Multiple cracks	Mushroom cracks
Proposed	0.9	0.85	0.8	0.77
Canny	0.35	0.99	0.96	0.27
Otsu	0.57	0.64	0.99	0.96

To measure the "goodness" of the threshold, a criterion is introduced by Otsu:

$$\eta = \frac{\sigma_B^2}{\sigma_T^2} \tag{10}$$

where $\sigma_B^2 = \omega_0(\mu_0 - \mu_T)^2 + \omega_1(\mu_1 - \mu_T)^2$ is the between-class variance and $\sigma_T^2 = \sum_{v=0}^{V-1}(v - \mu_T)^2 P_v$ is the total variance.

We search for the optimal threshold k, which maximizes η, and then perform global thresholding to obtain the final binary image.

5. Experimental results

We have tested the proposed crack detection filters by applying them to a variety of segmented underground pipe crack images and compared the results with those obtained by using the Canny's edge detection and the Otsu's thresholding technique.

5.1. Visual comparisons

Examples of the three approaches are shown in Figs. 10–12. It can be observed that the proposed filters perform better than the Canny's method and the Otsu's technique for detection of various kinds of cracks in underground pipe images.

The second and third rows in Figs. 10–12 show some minor and major cracks. The proposed algorithm performs well [Fig. 10(c)], detecting most of the minor and major crack structures in the images, while missing only the micro-cracks (second row) that experts in the pipe industry feel do not cause any structural problem.

The fourth row has a dark background with multiple cracks. In this case, the crack detection step performed well, but the results are noisy with a few false alarms. The cleaning and linking operations clearly show their effectiveness, able to fill gaps between the detected segments, providing a good map of the pipe surface, while suppressing most of the false alarms. In fact, the results are close to those that could be obtained by a trained human operator.

Table 4
Comparison under correctness metric (ideal response=1)

Methods	Minor cracks	Major cracks	Multiple cracks	Mushroom cracks
Proposed	0.99	0.98	0.94	0.93
Canny	0.52	0.29	0.41	0.65
Otsu	0.15	0.06	0.37	0.35

Table 5
Comparison under quality metric (ideal response=1)

Methods	Minor cracks	Major cracks	Multiple cracks	Mushroom cracks
Proposed	0.89	0.84	0.76	0.73
Canny	0.37	0.29	0.4	0.25
Otsu	0.14	0.06	0.38	0.36

The last row in Figs. 10–12 has a combination of many minor and major cracks (typically called a mushroom crack) with patches in the background. In this case the crack detection step performs less well, with many false-alarm responses. The performance evaluation of mushroom cracks is not easy because it is difficult even for human operators to track them. Nevertheless, the detection of a profusion of cracks, correlated with truth, is immediately apparent in Fig. 10(c).

5.2. Performance measure comparison

The following performance measures for crack extraction are intended to compare the results of different crack detection techniques, rather than to evaluate the extraction and the matching results in an absolute way, but giving a more quantitative and less subjective comparison than visually.

5.2.1. Completeness

$$\begin{aligned}\text{Completeness} &= \text{length of matched reference} \\ &\quad / \text{length of reference} \\ &\approx \frac{S_3}{S_3 + S_4} \quad \text{Completeness} \in [0, 1]\end{aligned} \tag{11}$$

The completeness is the percentage of the reference data that is explained by the extracted data, i.e., the percentage of the reference network that lies within the buffer around the extracted data. The optimum value for the completeness is 1.

5.2.2. Correctness

$$\begin{aligned}\text{Correctness} &= \text{length of matched extraction} \\ &\quad / \text{length of extraction} \\ &\approx \frac{S_1}{S_1 + S_2} \quad \text{Correctness} \in [0, 1]\end{aligned} \tag{12}$$

The correctness represents the percentage of correctly extracted crack data, i.e., the percentage of the extracted data that lies within the buffer around the reference network. The optimum value for the correctness is 1.

Table 6
Comparison under redundancy metric (ideal response=0)

Methods	Minor cracks	Major cracks	Multiple cracks	Mushroom cracks
Proposed	0	−0.01	0	0.02
Canny	0.24	−1.45	0.54	0.091
Otsu	−1.41	−1.72	−0.25	−0.31

5.2.3. Quality

$$\begin{aligned}\text{Quality} &= \text{length of matched extraction} \\ &\quad /(\text{length of extraction} \\ &\quad + \text{length of unmatched extraction}) \\ &\approx \frac{S_1}{S_1+S_2+S_4} \quad \text{Quality} \in [0,1]\end{aligned} \tag{13}$$

The quality is a more general measure of the final result combining completeness and correctness into a single measure. The optimum value for quality is 1.

5.2.4. Redundancy

$$\begin{aligned}\text{Redundancy} &= (\text{length of matched extraction} \\ &\quad - \text{length of matched reference}) \\ &\quad /\text{length of matched extraction} \\ &\approx \frac{S_1 - S_3}{S_1} \quad \text{Redundancy} \\ &\in [-\infty, +\infty]\end{aligned} \tag{14}$$

The redundancy represents the percentage, to which the correct (matched) extraction is redundant, i.e., it overlaps itself. The optimum value for the redundancy is 0.

The experimental results of performance measures are summarized in Tables 3–6. The performance of the proposed method is strikingly higher than the Canny or Otsu methods, particularly with respect to the latter three criteria, and is consistent with the visual results of Figs. 10–12.

6. Conclusions

The crack detection filters proposed in this paper can be simply divided into three steps: the crack detection filters D_1 and D_2 are used to extract cracks by taking into account the statistical properties of pixels within a small neighborhood; then the responses from both detectors are merged to obtain a unique response as well as an associated direction at each pixel; finally, the detection results are post-processed by cleaning and linking operations to provide crack segments.

In this paper a methodology for the evaluation of automatic crack detection filters based on the comparison to manually plotted reference data is presented. The proposed evaluation scheme captures the characteristics of the individual detection results and can thus serve as a basis for comparison. Depending on the application at hand, some of the quality measures may be more relevant than others (details can be found in [25]).

Comparing the proposed crack detection filters and the conventional detection techniques (i.e., Canny's and Otsu's), greatly improved experimental results has been achieved by the proposed statistical filters. The crack filters process along four directions over windows of increasing size and followed by cleaning and linking operations and can detect minor cracks (with small windows) as well as major cracks (with larger windows). The overall performance of proposed crack detection filters is found to perform well for underground pipe images with minor, major, and multiple cracks. Images with mushroom cracks are not detected as well, and although the performance evaluation of mushroom cracks is not easy because of the difficulty for human operators to establish ground truth, the results in Table 3 are quite promising.

References

[1] S.K. Sinha, P.W. Fieguth, Segmentation of buries concrete pipe images, Autom. Constr. (in press).

[2] L. Li, P. Chan, A. Rao, R.L. Lytton, Flexible pavement distress evaluation using image analysis, Proc. 2nd Intl. Conf on Transp. Engrg. (1991) 473–477.

[3] C. Haas, C. Hendrickson, Computer-based model of pavement surfaces, Transp. Res. Rec., 1260, Transp. Res. Board, Washington, DC (1990) 149–157.

[4] M.H. Mohajeri, P.J. Manning, ARIA: An operating system of pavement distress diagnosis by image processing, Transp. Res. Record 1311 (1991) 120–130.

[5] H.N. Koutsopoulos, A.B. Downey, Primitive based classification of pavement cracking images, J. Transp. Eng., ASCE 119 (3) (1993) 402–418.

[6] O. Moselhi, T. Shehab-Eldden, Automated detection of defects in underground sewer and water pipes, Autom. Constr. 8 (5) (1999) 581–588.

[7] O. Moselhi, T. Shehab-Eldden, Classification of defects in sewer pipes using neural networks, J. Infrastruct. Syst. 6 (3) (2000) 97–104.

[8] M.J. Chae, D.M. Abraham, Neuro-approaches for sanitary sewer pipeline condition assessment, J. Comput. Civ. Eng. 15 (1) (2001) 4–14.

[9] E. Nezry Lopes, R. Touz, H. Laur, Structure detection, and statistical adaptive filtering in SAR images, Int. J. Remote Sens. 14 (9) (1993) 1735–1758.

[10] Y. Yakimovsky, Boundary and object detection in real world images, J. Assoc. Comput. Mach. 23 (1976) 599–618.

[11] J. Skingley, A.J. Rye, The hough transform applied to images for thin line detection, Pattern Recogn. Lett. 6 (1987) 61–67.

[12] C.S. Regazzoni, G.L. Foresti, S.B. Serpico, An adaptive probabilistic model for straight edge extraction, Proc. IGARSS, Italy (1995) 458–460.

[13] O. Hellwich, H. Mayer, G. Winkler, Detection of lines in synthetic aperature radar (SAR) scenes, Proc. ISPRS 31 (1996) 312–320 (Vienna).

[14] I. Bloch, Information combination operators for data fusion: a comparitive review with classification, IEEE Trans. Syst. Man Cybern. 26 (1996) 52–67.

[15] A. Farag, E. Delp, Edge linking by sequential search, Pattern Recogn. 28 (5) (1995) 611–633.

[16] T. Law, H. Itoh, H. Seki, Image filtering, edge detection, and edge tracing using fuzzy reasoning, IEEE Trans. Pattern Anal. Mach. Intell. 18 (1996) 481–491.

[17] Q. Zhu, M. Payne, V. Riordan, Edge linking by a directional potential function, Image Vis. Comput. 14 (1) (1996) 59–70.

[18] P.C. Palmer, K. Kittler, M. Petrou, Using of attention with the hough transform for accurate line parameter estimation, Pattern Recogn. 27 (9) (1994) 1127–1134.

[19] D. Geman, S. Geman, C. Graffigne, P. Dong, Boundary detection by constrained optimization, IEEE Trans. Pattern Anal. Mach. Intell. 12 (1990) 609–628.

[20] J. Porrill, Fitting ellipse and predicting confidence envelopes using a bias correction Kalman filter, Image Vis. Comput. 8 (1) (1990) 37–41.
[21] R.O. Duda, P.E. Hart, Pattern Classification and Scene Analysis, Wiley Publication, New York, 1970, pp. 271–272.
[22] C. McGlone, J. Shufelt, Projective and object space geometry for monocular building extraction, Comput. Vis. Pattern Recogn. (1994) 54–61.
[23] J.F. Canny, A computational approach to edge detection, IEEE Trans. Pattern Anal. Mach. Intell. 8 (6) (1986) 679–698.
[24] N. Otsu, A threshold selection method from gray-scale histogram, IEEE Trans. Syst. Man Cybern. 9 (1) (1979) 62–66.
[25] S.K. Sinha, Automated underground pipe inspection using a unified image processing and artificial intelligence methodology. Ph.D. Thesis, University of Waterloo (2000).